

## Modelling

# Effects of depth-dependent properties on the thermal anomalies produced in flush instabilities from phase transitions

Volker Steinbach <sup>a,\*</sup>, David A. Yuen <sup>b</sup>

<sup>a</sup> *Institut fuer Geophysik und Meteorologie, Universitaet zu Koeln, D-50923 Koeln, Germany*

<sup>b</sup> *Minnesota Supercomputer Institute and Department of Geology and Geophysics, University of Minnesota, Minneapolis, MN 55415, USA*

Received 13 August 1993; accepted 21 February 1994

---

### Abstract

The effects of depth-dependent thermal expansivity, viscosity and thermal conductivity on mantle convection with phase transitions have been examined with two-dimensional finite-element simulations in an aspect-ratio four box. The model includes a core–mantle thermal coupling boundary condition which takes into play the secular cooling of the core by the overlying mantle flow. Initial surface Rayleigh numbers between  $2 \times 10^7$  and  $10^8$  have been considered. With time the surface Rayleigh number decreases to a value upon which a transition takes place from layered to single-cell convection. This tumultuous period is marked by large-scale coherent breakthrough of cold material, trapped in the transition zone, all the way to the base of the mantle and a violent reaction of hot plume in the upper mantle. Both hot and cold anomalies have large magnitudes. Cold anomalies with temperatures exceeding 1000 K are found at the base of the mantle. The magnitude of the cold anomalies is largest with all three depth-dependent properties. The timescales of this catastrophic event are between 20 and 50 Myr, with the longest being produced by the model with depth-dependent expansivity and viscosity. Results from these simple two-dimensional cartesian models represent a lower bound to the larger cold thermal anomalies, potentially capable of being generated in spherical-shell convection models.

---

### 1. Introduction

In the last year we have witnessed the appearance of one of the most exciting and significant problems to be recognized by geodynamicists in many years. This is the ‘flush’ event caused by strong gravitational instabilities developed in the transition zone (Weinstein, 1993; Steinbach and

Yuen, 1992; Honda et al., 1993; Steinbach et al., 1993; Tackley et al., 1993; Solheim and Peltier, 1994). These studies indicate that mantle convection today might be intermittent between a two-layer mode and a whole-mantle mode. The transition from the two-layer mode to the whole-mantle mode would occur via a rapid discharge of cold material on top of the 670 km phase change into the lower mantle. Although the works listed above have brought out some of the effects of this spectacular instability, there remains a great deal to learn about this important phenomenon.

---

\* Corresponding author.

This instability has implications concerning the dynamics of the lower mantle, because the locations of very cold material in the lower mantle today, as imaged by seismic tomography (Su and Dziewonski, 1992) and converted to thermal anomalies by mineral physics (Yuen et al., 1993; Cadek et al., 1994) can reveal a great deal about the style of time-dependent mantle convection in the presence of phase transitions. The very precarious and leaky character of the 670 km boundary has also important implications for the usage of normal-mode analysis in postglacial rebound and rotational dynamics problems (e.g. Spada et al., 1992; Ricard et al., 1993) because of the laterally varying conditions likely to exist in the vicinity of the 670 km discontinuity.

The dynamical importance of depth-dependent properties on mantle flows and thermal structure has been brought out in recent papers by Hansen et al. (1991, 1993) and Balachandar et al. (1992, 1993). In this paper we will explore the effects of depth-dependent properties on the thermal structures as a consequence of dump-like instabilities caused by phase transitions. The depth dependences of thermal expansivity, viscosity and thermal conductivity will be considered in increasing order of combinations. We regard this as a first step in quantifying the thermal anomalies associated with these flushing events. Cadek et al. (1994) have found very cold anomalies in the deep mantle under past subducting sites by converting the seismic anomalies using mineral physics data. This work attempts to reconcile these cold anomalies from a modelling perspective. We will also monitor the hot thermal anomalies which are generated during this flush instability, as there might be a relationship between the rapid subduction rates during the Cretaceous and superplume events (Larson, 1991).

## 2. Mathematical formulation and model description

We treated the equations of conservation of mass, momentum and energy for an infinite Prandtl number fluid in the extended Boussinesq approximation (Christensen and Yuen, 1985),

where density variations owing to temperature gradients and/or phase changes are explicitly accounted for only in the buoyancy term that drives the convective flow. Additionally, the non-Boussinesq effects of viscous dissipation and adiabatic heating and cooling are incorporated as well as the release (or consumption) of latent heat owing to phase transitions.

The validity and limitations of this approach for flows without phase transitions have been discussed by Steinbach et al. (1989). For convection with phase changes, it means that the flow is considered to be incompressible even in the phase-transition region, but that the (vertical) distortion of the phase boundaries owing to horizontal temperature gradients (which is proportional to the Clapeyron slope of the transition) is accounted for. In the presence of an endothermic phase transition (with negative Clapeyron slope), it is this distortion which has the most profound effect on the convective flow pattern, as it acts as a barrier to both cool downwelling and hot upwelling masses and thus may cause layered convection. As we want to compare how the depth dependence of several parameters affects the mass exchange between upper and lower layer in an initially stably stratified convective system, we believe that application of the extended Boussinesq approximation will capture the most important facets of the physics in such systems, even though it is not justified in a strictly mathematical sense.

As our derivation of the nondimensional equations governing convective flows with phase transitions up to Eq. (17) closely follows the approach of Christensen and Yuen (1985), we will present it only briefly and refer the reader to that paper for further details. For each phase transition, we introduce a phase function  $\Gamma_i$ , ( $i = 1, \dots, n$ ), which gives the fraction of the denser phase and hence varies between zero and unity as a function of the 'excess pressure' alone (Christensen and Yuen, 1985):

$$\pi = p - p_{0i} - \gamma_i T [D] \quad (1)$$

where  $p$  and  $T$  are pressure and temperature, and  $p_{0i}$  and  $\gamma_i$  are zero-degree transition pressure and Clapeyron slope of the  $i$ th phase transi-

tion, respectively. Henceforth, the equations with a bracketed  $D$  represent dimensional quantities. In our models we investigate rather sharp transitions. The extent of the region where  $\Gamma_i$  deviates appreciably from zero and unity is small compared with the depth of the convective layer, and the explicit dependence of  $\Gamma_i$  on  $\pi$  is of little significance (Richter, 1973). Here we will just state that owing to the sharpness of the transitions  $d\Gamma_i/d\pi$  peaks at  $\pi = 0$  and rapidly vanishes outside the transition region.

To calculate the buoyancy forces owing to temperature variations and phase transitions we use a first-order equation of state:

$$\rho = \rho_0 \left[ 1 - \alpha(T - T_0) + \sum_{i=1}^n \frac{\Delta\rho_i}{\rho_0} \Gamma_i \right] [D] \quad (2)$$

where  $\rho$  denotes density,  $\alpha$  thermal expansivity, and  $\Delta\rho_i$  the density jump owing to the  $i$ th phase transition. Subscripts zero denote surface values.

Introducing the streamfunction  $\psi$  and the  $y$  component of vorticity  $\omega$  as

$$\left( \frac{\partial\psi}{\partial z}, 0, -\frac{\partial\psi}{\partial x} \right) = (u, 0, w)$$

$$\omega = \frac{\partial u}{\partial z} - \frac{\partial w}{\partial x}$$

where  $u$  and  $w$  denote respectively the horizontal and vertical velocities, and scaling spatial quantities by the depth of the layer,  $h$ , pressure by  $\rho_0 gh$  (where  $g$  is gravitational acceleration), temperature by the temperature difference across the layer,  $\Delta T$ , the Clapeyron slopes by  $\rho_0 gh/\Delta T$  and time by  $h^2/\kappa_0$  (where  $\kappa_0$  is thermal diffusivity), we obtain the dimensionless equations for conservation of mass and momentum, appropriate for depth-dependent viscosity and thermal expansivity:

$$\nabla^2\psi = \omega \quad (3)$$

$$\nabla^2(\eta\omega) = \alpha\text{Ra} \frac{\partial T}{\partial x} - \sum_{i=1}^n \text{R}_{bi} \frac{\partial\Gamma_i}{\partial x} + 2 \frac{\partial^2\psi}{\partial x^2} \frac{\partial^2\eta}{\partial z^2} \quad (4)$$

Neglecting the nonhydrostatic pressure in the dimensionless form of (1),

$$\pi = z_{0i} - z - \gamma_i T \quad (5)$$

(the  $z$ -axis pointing upwards) and making use of the relationship

$$\frac{\partial\Gamma}{\partial x} = \frac{d\Gamma}{d\pi} \frac{\partial\pi}{\partial x} = -\gamma \frac{d\Gamma}{d\pi} \frac{\partial T}{\partial x} \quad (6)$$

we may rewrite (4) as

$$\nabla^2(\eta\omega) = \bar{\alpha}\text{Ra} \frac{\partial T}{\partial x} + 2 \frac{\partial^2\psi}{\partial x^2} \frac{\partial^2\eta}{\partial z^2} \quad (7)$$

Both thermal expansivity and dynamic viscosity  $\eta$  are allowed to vary with depth in our model and are scaled by their surface values. In this study we will choose  $\eta$  to vary linearly with depth, so the last term on the right-hand side of (7) vanishes. The parameters in (4)–(7) are the thermal Rayleigh number

$$\text{Ra} = \frac{\alpha_0 \rho_0 g \Delta T h^3}{\kappa_0 \eta_0} \quad (8)$$

the phase-boundary Rayleigh numbers

$$\text{R}_{bi} = \frac{\Delta\rho_i g h^3}{\kappa_0 \eta_0} \quad (9)$$

the effective thermal expansivity

$$\bar{\alpha} = \alpha + \sum_{i=1}^n P_i \frac{d\Gamma_i}{d\eta} \quad (10)$$

and the ‘phase-transition parameters’

$$P_i = \gamma_i \frac{\text{R}_{bi}}{\text{Ra}} \quad (11)$$

The rate of latent heat release per unit volume during each phase transition is given by

$$Q_i = \frac{\gamma_i T_a \Delta\rho_i}{\rho_0} \frac{D\Gamma_i}{Dt} [D] \quad (12)$$

where  $T_a$  is absolute temperature and  $D/Dt = \partial/\partial t + \mathbf{u} \cdot \nabla$ . Incorporating this into the dimensionless energy equation scaled the same way as in (3) and (7), and using the relationship

$$\frac{D\Gamma_i}{Dt} = -\frac{d\Gamma_i}{d\pi} \left( \gamma_i \frac{DT}{Dt} - \frac{\partial\psi}{\partial x} \right) \quad (13)$$

yields

$$\begin{aligned} \bar{C}_p \frac{DT}{Dt} - \bar{\alpha} D_0 (T + T_0) \frac{\partial\psi}{\partial x} \\ = \nabla(k\nabla T) + \frac{D_0}{\text{Ra}} \Phi + \frac{\text{Ra}_Q}{\text{Ra}} \end{aligned} \quad (14)$$

New quantities are the dissipation number

$$D_0 = \frac{\alpha_0 g h}{C_p} [D] \quad (15)$$

where  $C_p$  is specific heat (assumed to be constant), the dissipation function

$$\Phi = \sigma_{ij} \frac{\partial u_i}{\partial x_j} \quad (16)$$

the Rayleigh number owing to internal heat sources

$$\text{Ra}_Q = \frac{\alpha_0 \rho_0 g Q h^5}{\kappa_0^2 \eta_0 C_p} [D] \quad (17)$$

where  $Q$  is the internal heating rate and the effective specific heat

$$\bar{C}_p = 1 + D_0(T + T_0) \sum_{i=1}^n \gamma_i P_i \frac{d\Gamma_i}{d\pi} \quad (18)$$

$T_0$  denotes nondimensional surface temperature. Thermal conductivity  $k$  is scaled by its surface value and is allowed to vary with depth.

For the reader's convenience, we will rewrite the extended Boussinesq approximation of the constitutive equations with  $\eta$  linearly dependent on depth:

$$\nabla^2 \psi = \frac{\bar{\omega}}{\eta} \quad (19)$$

$$\nabla^2 \bar{\omega} = \bar{\alpha} \text{Ra} \frac{\partial T}{\partial x} \quad (20)$$

$$\begin{aligned} \bar{C}_p \frac{DT}{Dt} - \bar{\alpha} D_0 (T_0 + T) \frac{\partial \psi}{\partial x} \\ = \nabla(k \nabla T) + \frac{D_0}{\text{Ra}} \Phi + \frac{\text{Ra}_Q}{\text{Ra}} \end{aligned} \quad (21)$$

where we have introduced the modified vorticity,  $\bar{\omega} = \eta \omega$  (Turcotte et al., 1973). It is obvious that Eqs. (19)–(21) have the same form as the equations for convection without phase transitions with depth- and temperature-dependent thermal expansivity and specific heat. It should be noted that  $\bar{C}_p$  increases in each phase-transition region, whereas  $\bar{\alpha}$  may become negative in an endothermic phase transition (with negative Clapeyron slope) and act as a source of negative buoyancy

and latent heat for a rising plume. For Earth-like parameters, referring to the exothermic (positive  $\gamma$ ) olivine  $\rightarrow$  spinel and the endothermic (negative  $\gamma$ ) spinel  $\rightarrow$  perovskite transitions,  $|\gamma| \approx 0.1$  and  $|P| \approx 0.06$ . The peak value of  $d\Gamma/d\pi$  increases with the sharpness of the transition, i.e. with decreasing half-width  $d$  of the transition and can be rather large.

As the 'anomalous'  $\bar{C}_p$  (i.e. the second term of the right-hand side of (18)) scales with  $\gamma P$ , whereas the 'anomalous'  $\bar{\alpha}$  scales with  $P$  alone, it is obvious that the changes of  $\bar{\alpha}$  in the transition regions are much more (one order of magnitude) important effects than the changes in  $\bar{C}_p$ . Therefore we adopt  $\bar{C}_p \equiv 1$  in our model, thus reducing computational effort. For computational reasons it is also very convenient to neglect the temperature dependence of  $d\Gamma/d\pi$ , hence letting  $\bar{\alpha}$  be a function of depth alone. In a physical way, this means that we include the buoyancy effects owing to the distortion of the phase boundary, but neglect the distortion itself. Christensen and Yuen (1985) have shown that this procedure ( $\bar{C}_p \equiv 1$ ,  $\bar{\alpha} = \bar{\alpha}(z)$ ) is a very good approximation to the full set of equations, as far as the amount of layering and the transition from layered to non-layered flows is concerned. Because in this paper we will focus just on this last point, it is justified to adopt the above approximation for this comparative study.

As mentioned above, the exact form of  $d\Gamma/d\pi$  is of little significance, as long as it peaks in the middle of the transition region and rapidly flattens outside this region. We made the following ansatz for  $\bar{\alpha}$ :

$$\bar{\alpha} = \alpha(z) + \sum_{i=1}^2 A_i f_i(\bar{z}) \quad (22)$$

with

$$\bar{z} = \min\left(\left|\frac{z - z_{0i}}{d_i}\right|, 1\right) \quad (23)$$

and

$$f_i(\bar{z}) = 1 - 2\bar{z}^2 + \bar{z}^4 \quad (24)$$

where  $z_{0i}$  and  $d_i$  are the depths and half-widths of the phase transitions. Other forms of  $f(z)$ ,

such as Gaussian (Honda et al., 1993), can be used with virtually no difference. The index 1 refers to the olivine → spinel, and the index 2 refers to the spinel → perovskite transition, yielding positive  $A_1$  and negative  $A_2$ . As

$$\int_0^1 \frac{d\Gamma}{d\pi} d\pi \equiv 1 \quad (25)$$

the amplitudes  $A_i$  of the ‘anomalous’  $\bar{\alpha}$  are inversely proportional to the half-widths of the transitions:

$$A_i = \frac{15 P_i}{16 d_i} \quad (26)$$

As stated above, the ‘background’ thermal expansivity  $\alpha(z)$  in (22), thermal conductivity  $k$  and dynamic viscosity  $\eta$  generally are allowed to be functions of depth in our model. We chose the following functional dependences for these quantities:

$$\alpha(z) = (2 - z)^{-3} \quad (27)$$

$$k(z) = (2 - z)^{3/2} \quad (28)$$

$$\eta(z) = 1 + 9(1 - z) \quad (29)$$

which results in bottom/top ratios of 1/8, 2.83 and 10, respectively. Eq. (27) fits rather well the depth variations of  $\alpha$  obtained from laboratory experiments (Chopelas and Boehler, 1992). Eq. (28) comes from the phonon contribution to thermal conductivity (Anderson, 1987).

### 2.1. Model description

We consider a model based on a cartesian geometry (see Fig. 1) with an aspect ratio of 4:1, with unity being the depth of the layer. To carry out a systematic study of time-dependent convection with phase changes, we had to reduce further the computational effort in solving Eqs. (19)–(21). We achieved this by restricting mantle depth to 2000 km (see Fig. 1) and choosing transition widths of 50 km ( $d = 0.025$ ). For Earth-like parameters (Ito and Takahashi, 1989; Ito et al., 1990; see Table 1), this gives  $A_i \approx \pm 2.5$ . To correct for the actually narrower phase-transition depths, we chose  $A_i = \pm 5$ , corresponding to a

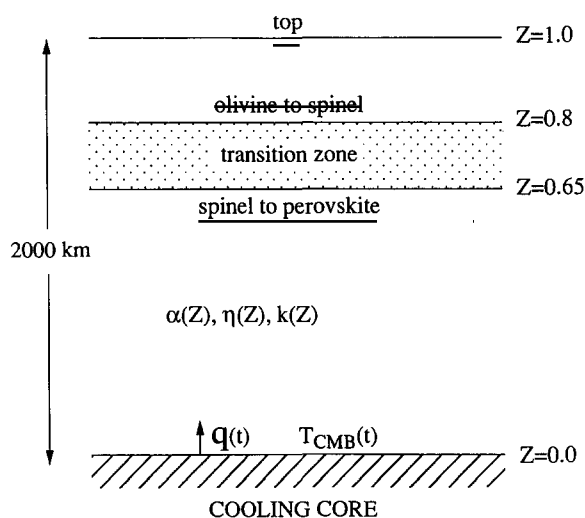


Fig. 1. Schematic diagram of the different depth ranges included in the numerical model. Both the olivine → spinel and spinel → perovskite phase transition are included at nondimensional depths of 0.8 and 0.65, respectively, for a mantle with 2000 km depth. The grid is refined in the top and bottom thermal boundary layers and in the transition zone. Thermal expansivity  $\alpha$ , conductivity  $k$  and dynamic viscosity  $\eta$  generally are functions of depth as given in Eqs. (27)–(29). At each time-step, the heat flux from the core  $q(t)$  is calculated and the new core temperature  $T_{\text{CMB}}(t)$  is evaluated according to Eq. (34).

half-width of 25 km, without actually reducing  $d$ . We are fully aware of the fact that there are strong limitations in this procedure when applied to the real Earth, but again we wish to stress that it is our aim to carry out a comparative study of the transition from layered to non-layered convection with different depth dependences of some parameters. Hence the results must be interpreted from a qualitative point of view and cannot be strictly applied in a quantitative manner to planetary interiors.

Table 1  
Physical properties of the phase changes included

Quantity	Olivine → spinel	Spinel → perovskite
$\alpha_0$	$5.2 \times 10^{-5} \text{ K}^{-1}$	$5.2 \times 10^{-5} \text{ K}^{-1}$
$\Delta T$	2800	2800
$\Delta\rho/\rho_0$	0.08	0.1
$\gamma$	$3 \text{ MPa K}^{-1}$	$-2.5 \text{ MPa K}^{-1}$

We have solved Eqs. (19)–(21) with a finite element SUPG (Streamline Upwind Petrov Galerkin) scheme (e.g. Hansen and Ebel, 1984). We have used throughout 50 (vertical)  $\times$  200 (horizontal) elements for the aspect ratio four calculations. To guarantee that the ‘interesting’ regions are resolved adequately, we have refined our grid vertically to make sure that each thermal boundary layer and phase-transition region is covered by at least four elements.

As was pointed out by Christensen and Yuen (1985) and Steinbach et al. (1993), the degree of layering of convection with phase boundaries increases with Rayleigh number. It is a tedious task to investigate the amount and style of mass exchange between the two convective layers for a broad range of Rayleigh numbers with a time-dependent model. We have therefore decided to take into account that the Rayleigh number, as defined in (8), decreases with time as a result of secular cooling of core and mantle. In this way, it is possible to study the character of the breakdown of layered convection that can be expected when the Rayleigh number approaches a certain critical value  $Ra_c$ , from above. In contrast to most of the previous models (Christensen and Yuen, 1985; Machetel and Weber, 1991; Zhao et al., 1992; Honda et al., 1993; Tackley et al., 1993), in which a constant-temperature boundary condition has been assumed at the core–mantle boundary (CMB), we take into account core cooling owing to mantle convection by adapting a simple model. This change of boundary condition brings in the possibilities for strong non-equilibrium effects in the evolutionary dynamics of the mantle. We assume that the core is always in thermodynamic equilibrium (has infinite effective thermal conductivity) and is homogeneous (mean parameters for inner and outer core). The (dimensional) equation for the core’s cooling then is

$$\rho_c C_c \frac{dT_c}{dt} = -\text{div}(q_c) [D] \quad (30)$$

where  $\rho_c$  denotes mean core density (approximately  $12 \text{ g cm}^{-3}$ ),  $C_c$  is the core’s specific heat (approximately  $5 \times 10^2 \text{ J kg}^{-1} \text{ K}^{-1}$ ),  $T_c$  is the core’s temperature and  $q_c$  is the heat flux from the core.

In a spherical geometry, integration over the core’s volume yields

$$\frac{4}{3}\pi r_c^3 \rho_c C_c \frac{dT_c}{dt} = -4\pi r_c^2 q_c [D] \quad (31)$$

where  $r_c$ , the core radius, is  $3.485 \times 10^6 \text{ m}$ .

Introducing the dimensionless quantities Nusselt number  $Nu$  at the CMB and temperature difference  $\Delta T$  between the CMB and surface as

$$Nu = \frac{q_c d}{k_m (T_c - T_0)} \quad (32)$$

$$\Delta T = \frac{T_c - T_0}{T_c(t=0) - T_0} \quad (33)$$

with  $k_m$  and  $\kappa_m$  being mantle thermal conductivity and diffusivity, respectively, we obtain

$$\frac{d\Delta T}{dt} = -\frac{3\rho_m C_m d}{\rho_c C_c r_c} Nu(t) \Delta T(t) \quad (34)$$

where  $\rho_m$  (approximately  $5 \text{ g cm}^{-3}$ ),  $C_m$  (approximately  $1.25 \times 10^3 \text{ J kg}^{-1} \text{ K}^{-1}$ ) and  $d = 2.886 \times 10^6$  are mean density, specific heat and depth of the mantle, respectively. We note that  $Nu$  in Eq. (32) is calculated using the local properties. Time is scaled by thermal diffusion time. Using this scheme, we neglect the release of latent and gravitational heat owing to freezing of the inner core. However, Buffett et al. (1992) have shown that the ratio of heat production in the core and heat loss to the mantle is of order  $c/b$ , where  $c$  and  $b$  denote inner and outer core radii, respectively. With a present ratio of 0.35 it is clear that core cooling is the dominant process and was even more important in the Earth’s early stages. We intend to include the thermodynamics of the evolution of the inner core into our numerical scheme in the near future. As our models are cartesian, it is necessary to make the assumption that the large-scale patterns are similar to axisymmetric solutions. For depth-dependent thermal expansivity this has been shown by Leitch and Yuen (1991).

After each time-step, the new temperature difference is calculated from the Nusselt number with a simple Euler forward scheme of Eq. (34). The error related to the neglect of the variation of  $\Delta T$  during one time-step  $\delta t$  then is of order

$\delta t^2$ . The effects of varying Rayleigh number is most prominent when one considers temperature-dependent viscosity, as viscosity decreases from secular cooling could be as large as two to three orders of magnitude (Sharpe and Peltier, 1978). We take into account this dependence of effective viscosity on mean temperature of the form  $\nu_{\text{eff}} \sim \bar{T}^{-m}$ , where  $m$  is an integer of order ten (Davies, 1980). In the numerical treatment of

Eqs. (19)–(21) the readjustment of  $\Delta T$  and  $\nu_{\text{eff}}$  only changes the Rayleigh number according to

$$\frac{Ra_{n+1}}{Ra_n} = \frac{\Delta T_{n+1}}{\Delta T_n} \cdot \left( \frac{T_0 + \Delta T_{n+1} \bar{T}_{n+1}}{T_0 + \Delta T_n \bar{T}_n} \right)^m \quad (35)$$

where subscripts  $n$  and  $n + 1$  denote consecutive time-steps. As temperatures are rescaled by the new temperature difference after each time-step,

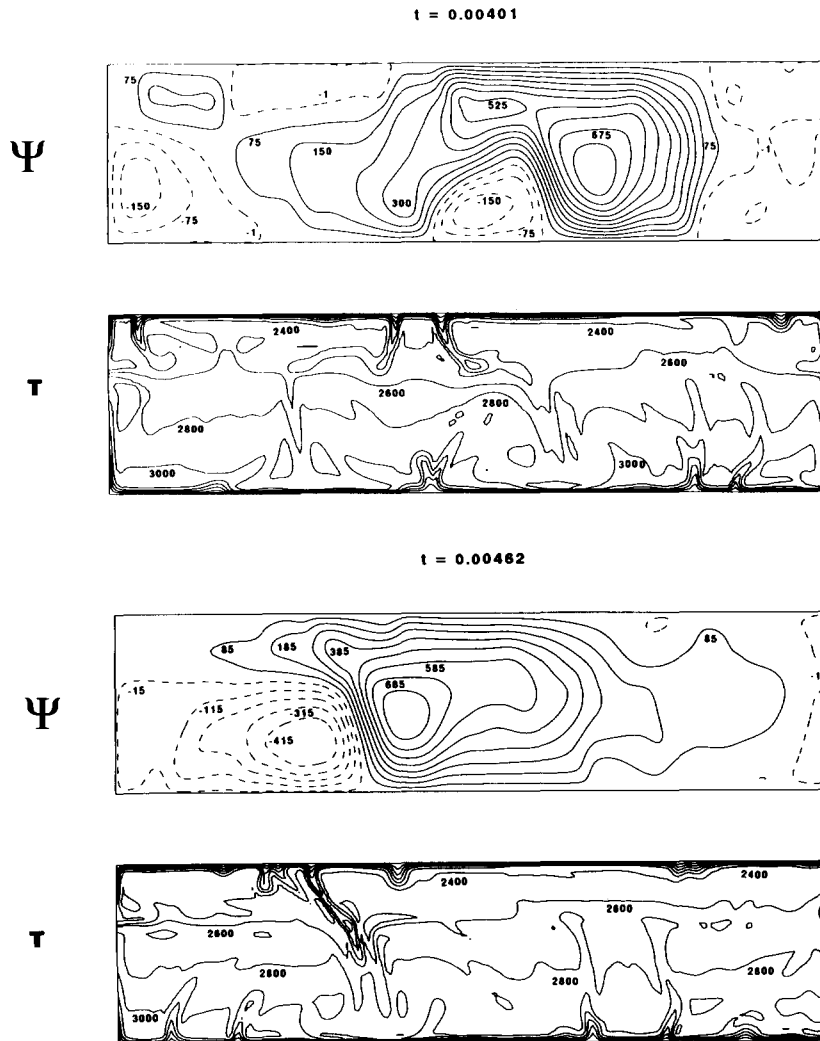


Fig. 2. Snapshots of streamlines ( $\Psi$ ) and isotherms ( $T$ ) of a flow with constant material properties and a constant core temperature  $T_{\text{CMB}}$  at a Rayleigh number of  $10^7$ . (Note that the streamlines at  $t = 0.00401$  indicate regions of whole-mantle convection as well as some layered structures.) We note that for this model 0.001 in time corresponds to 127 Myr.

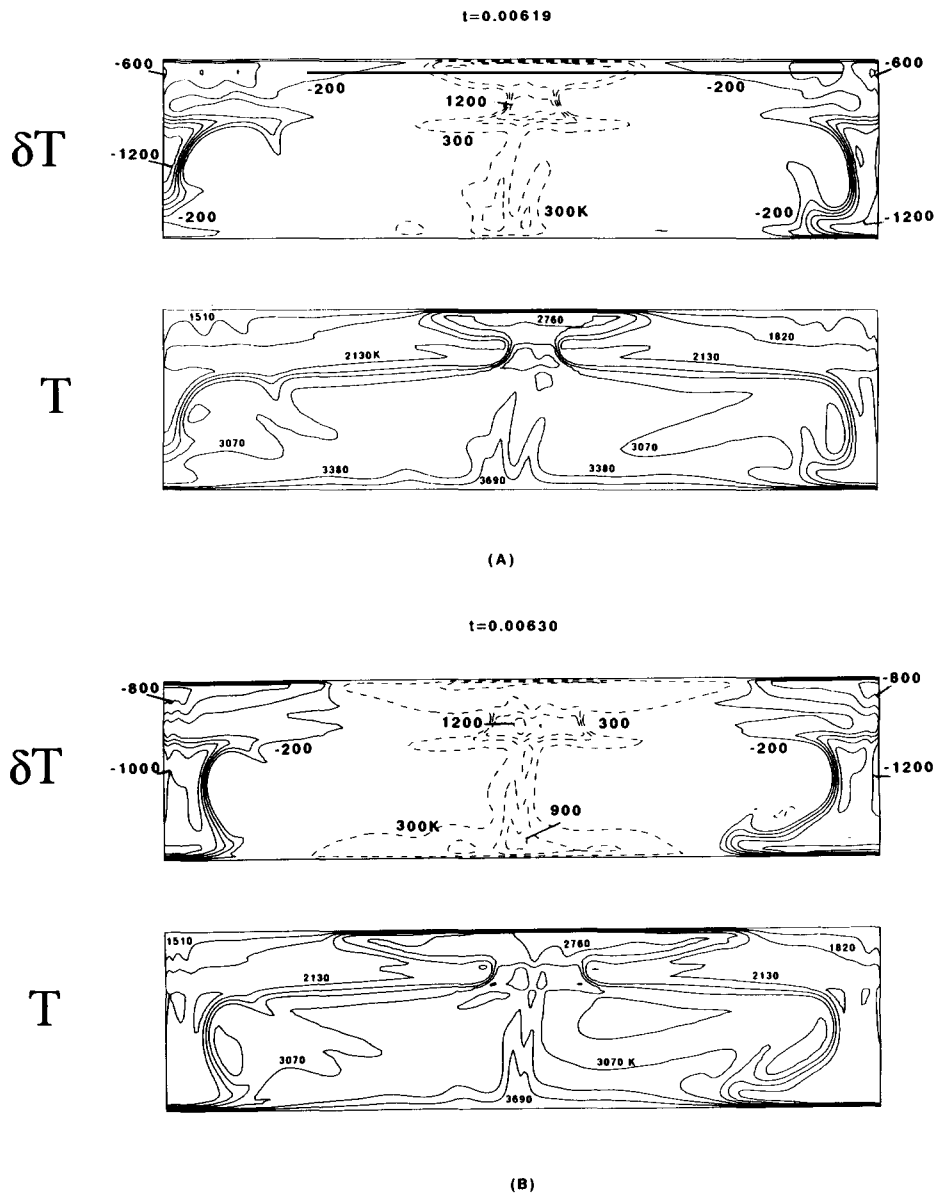


Fig. 3. Isotherms ( $T$ ) and lateral temperature anomalies ( $\delta T$ ) at three different time-steps during the 'flush' event. A model with depth-dependent thermal expansivity (cf. Eq. (27)) and constant thermal conductivity and viscosity was used. Initial condition was a layered flow at a surface Rayleigh number of  $Ra_0 = 2 \times 10^7$ . At each time-step core temperature and surface Rayleigh number were adjusted according to Eqs. (34) and (35). The transition from layered to non-layered flow takes place at  $Ra_0 \approx 4 \times 10^6$ . All dimensional temperatures were calculated by assuming a surface temperature of 1200 K and a core-mantle temperature of (initially) 4000 K.

dimensionless temperature values remain the same throughout the computation, whereas dimensional CMB temperature drops from 4000 to about 3700 K in a typical calculation.

### 3. Results

In this section we will discuss the results obtained in the order of increasing complexities of

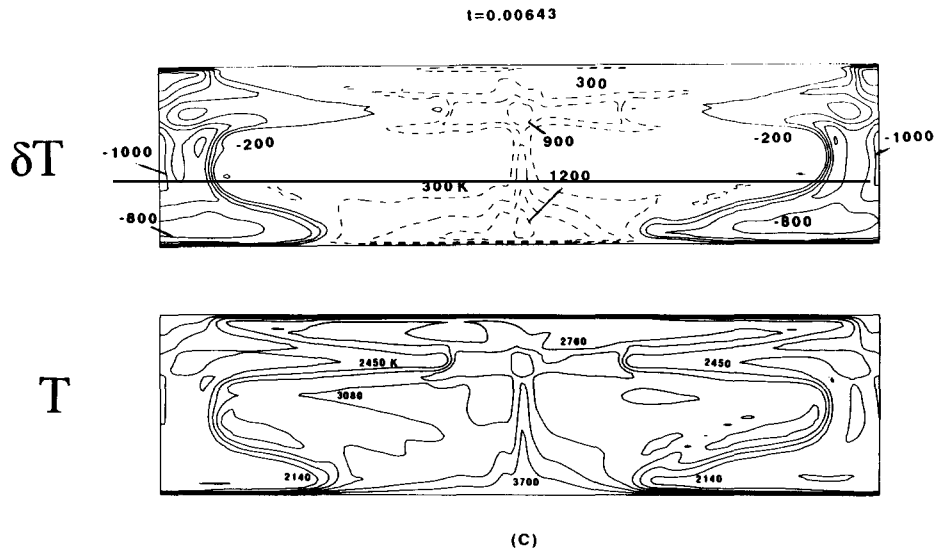


Fig. 3 (continued).

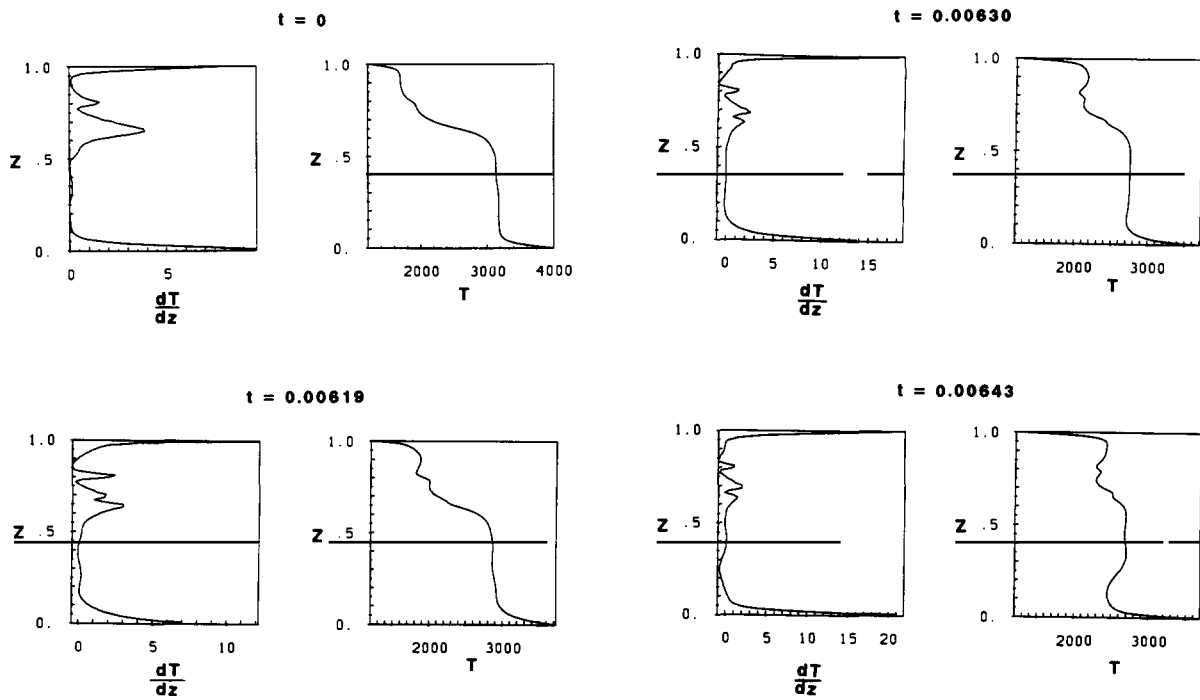


Fig. 4. Profiles of horizontally averaged temperature ( $T$ ) and temperature gradient ( $dT/dz$ ) of the initial flow and the three time-steps shown in Fig. 3. During the ‘flush’ event the initially strong internal thermal boundary layer is dissolved and a large subadiabatic region builds up in the lower mantle owing to the subduction of cold material.

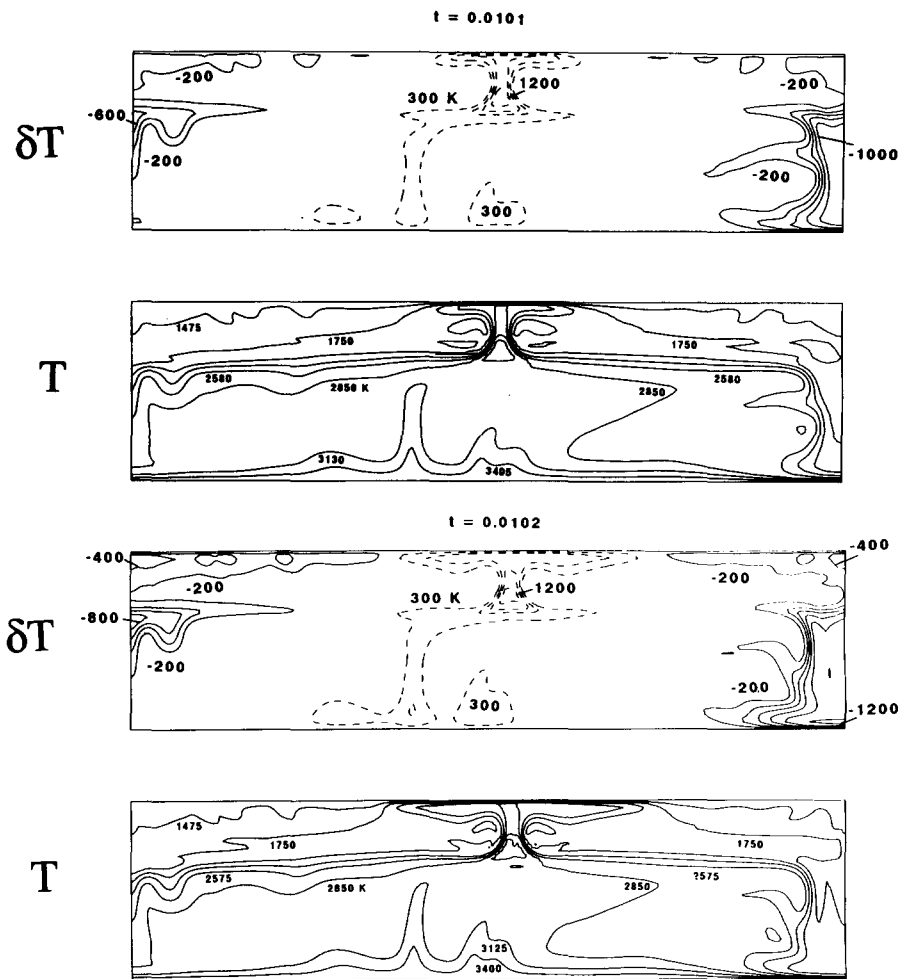


Fig. 5. Isotherms and lateral thermal anomalies at five different time-steps during the 'flush' event. The model includes both depth-dependent thermal expansivity and viscosity. Initial condition was a layered flow at a surface Rayleigh number of  $10^8$ . The transition from layered to non-layered flow took place at  $Ra_0 \approx 1.2 \times 10^7$ . Otherwise, all quantities are the same as in Fig. 3.

depth dependences. We begin with a constant-property model.

### 3.1. Constant properties

For models with constant physical properties we did not find a strongly layered solution for  $Ra \approx 10^7$  without any internal heating ( $Ra_Q = 0$ ). In this study we have taken  $Ra_Q = 0$  throughout. We show in Fig. 2 two snapshots of the streamfunction  $\Psi$  and the temperature field  $T$  for  $Ra = 10^7$  with a constant-temperature boundary condi-

tion at the base of the mantle. The streamlines show a complicated pattern and the temperature fields exhibit some blocking features in the neighbourhood of the transition zone between  $z = 0.6$  and  $z = 0.85$  (see Fig. 1). Unlike regular base-heated Newtonian convection one sees a strong lateral heterogeneity in the strength of the flow field from the localized nature of the interaction of the descending plume with the transition zone in the middle of the box. The descending flows can penetrate through the transition zone much easier than the ascending plumes can. The same

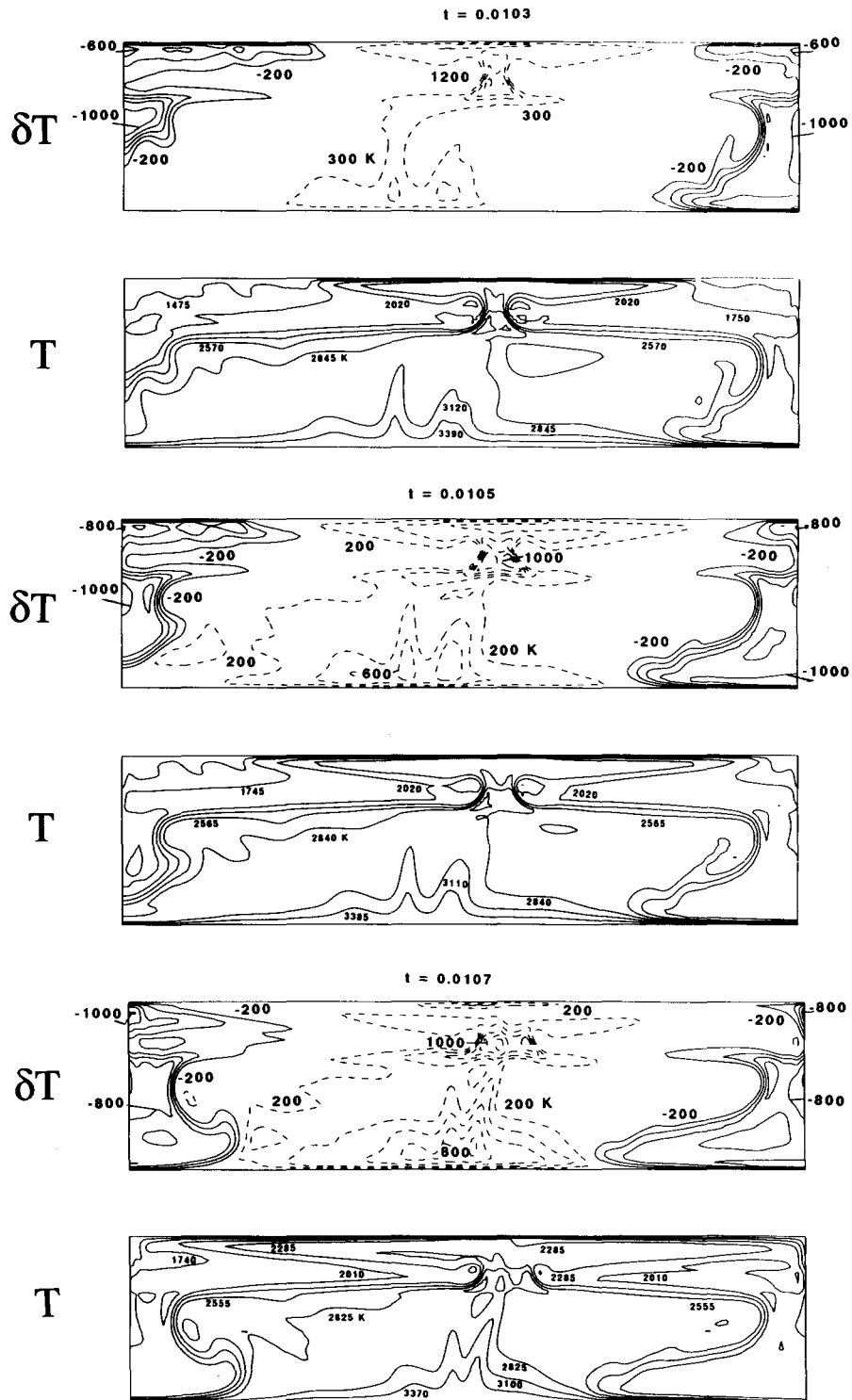


Fig. 5 (continued).

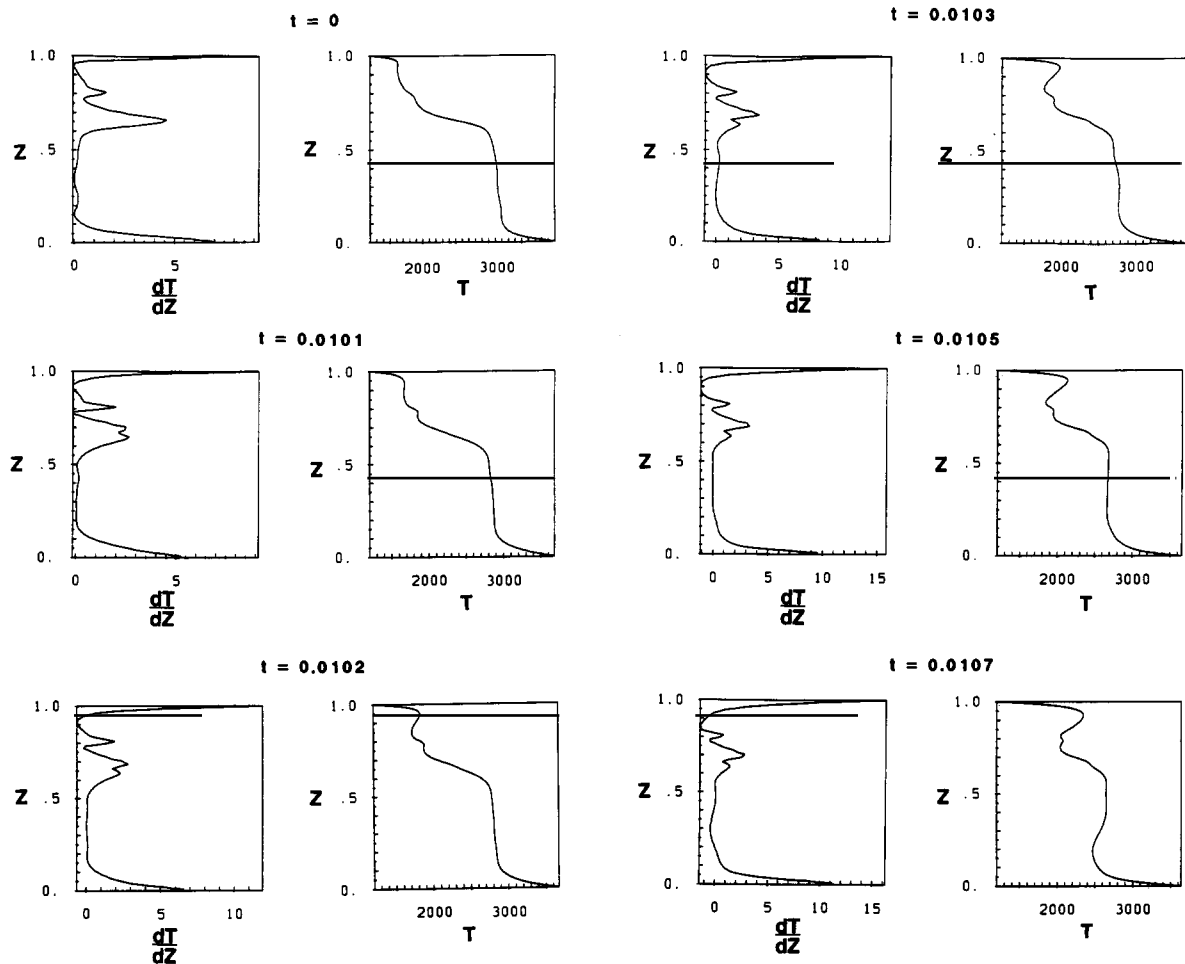


Fig. 6. Profiles of horizontally averaged temperature and temperature gradient of the initial flow and the five time-steps shown in Fig. 5. Behaviour in these profiles is found to be very similar to that in Fig. 4.

phenomenon has also been found by Machetel and Weber (1991) and Zhao et al (1992) for constant-property convection with phase transitions.

### 3.2. Depth-dependent expansivity

Models with depth-dependent thermal expansivity have been found to have a greater tendency for layered convection (Zhao et al., 1992). We have used a thermal expansivity which decreases by a factor of eight across the layer (see Eq. (27)). The initial state was taken from a layered convec-

tive state at  $Ra_0 = 2 \times 10^7$ . Then we applied the core-coupling boundary condition (eq. (34)) to this initial condition and began to integrate forward in time. The Rayleigh number of the system decreases because of the decrease of the CMB temperature and the overall increase of the effective viscosity (Eq. (35)) where  $m$  is taken to be 30. When the surface Rayleigh number  $Ra_0$  has decreased to about  $4 \times 10^6$ , which corresponds to a mean Rayleigh number  $\langle Ra \rangle$  of  $1.5 \times 10^6$ , a catastrophic instability takes place (Fig. 3). The rapid sinking of the cold instabilities also triggers paroxysmal reaction of the hot plumes (dashed

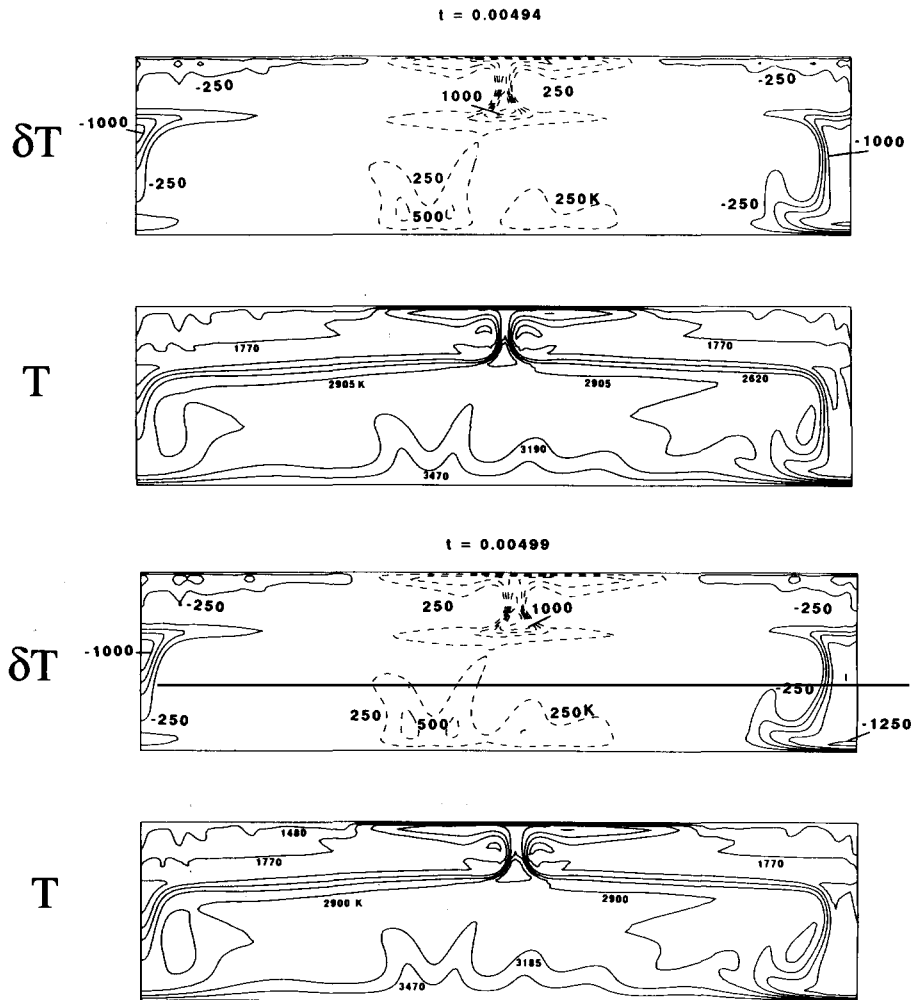


Fig. 7. Temperature and thermal anomaly fields at six different time-steps during the 'flush' event for a model with depth-dependent thermal expansivity, viscosity and thermal conductivity. Initial condition was the same as in Fig. 5. The transition from layered to non-layered flow occurred at  $Ra_0 \approx 2.2 \times 10^7$ . Otherwise, all quantities are the same as in Figs. 3 and 5.

curve). Cold lateral anomalies (solid curves in  $\Delta T$ ) exceeding 1000 K can reach the bottom. These anomalies are thick, and it takes some time for them to be eroded away. At the same time, very hot lateral anomalies (dashed curves in  $\Delta T$ ) are generated in the upper mantle above the 670 km discontinuity. This series of snapshots covers a span of around 30 Ma. In Fig. 4 we show the horizontally averaged vertical temperature gradient  $dT/dz$  and the horizontally averaged temperature  $T$  for four different panels, including the initial condition. The destruction of the lay-

ered structure by the flush event is clearly shown in these profiles. In the last panel ( $t = 0.00643$ ) we observe a negative slope in  $T$  near the CMB. This indicates strong subadiabaticity in the aftermath of a flush event and is due to the spreading of cold material at the base of the mantle.

### 3.3. Depth-dependent expansivity and viscosity

The depth variations in viscosity are generally believed to be greater than those of thermal expansivity. Hansen et al. (1993) have studied the

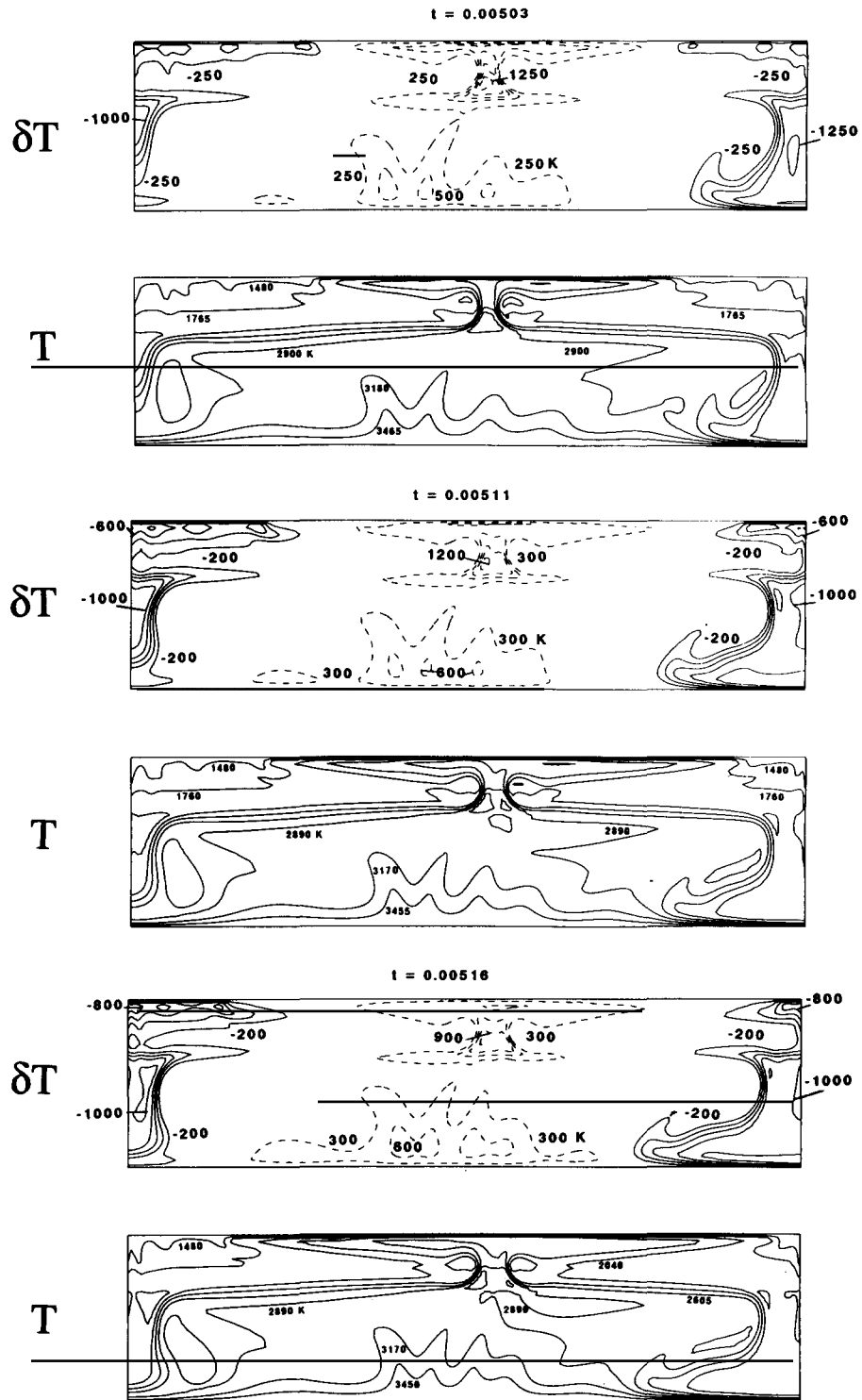


Fig. 7 (continued).

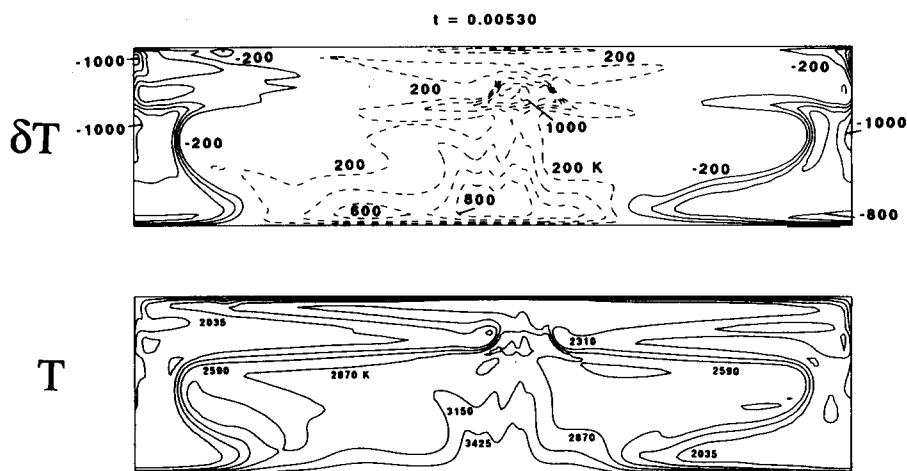


Fig. 7 (continued).

combined effects from these two depth dependences and found that, taken together, they can greatly reduce the mean interior temperature. We have used a linearly increasing viscosity with a contrast of ten across the layer in addition to the above thermal expansivity used in Fig. 3. The initial state was taken from a layered convective state at  $Ra_0 = 10^8$ . We then carried out the integration with the time-varying boundary condition for the temperature at the CMB. With both thermal expansivity and viscosity depth dependences the transitional surface Rayleigh number  $Ra_0$  at which the flushing event took place was found to be around  $1.2 \times 10^7$ , which was higher than the transitional  $Ra_0$  for depth-dependent thermal expansivity (Figs. 3 and 4), whereas the mean Rayleigh number  $\langle Ra \rangle$  was found to be  $8.2 \times 10^5$ , lower than that for the depth-dependent expansivity alone. Owing to the higher viscosity, the speed at which the flushing instability took place was about two times slower than in the case with the depth-dependent thermal expansivity (see Fig. 9 below). The duration of time shown in the temperature panels is 65 Myr. Cold anomalies, sometimes exceeding 1000 K, were able to plunge down to the bottom of the mantle (Fig. 5). There was a continuous eruption of hot anomalies in the upper mantle. Very hot anomalies, exceeding 1000 K above the ambient, occurred. These events would lead to extensive melting in the upper

mantle and periods of intense volcanism, characteristic of the superplume event in the Cretaceous (Larson, 1991), when there was a large build-up of basalt volcanism. The isotherms in Fig. 5 indicate that the penetration of hot material into the upper mantle is not a consequence of a hot active plume rising from the CMB but rather is triggered by the ‘flush’ of the cold upper-mantle masses. Modelling efforts by Weinstein (1993) and Honda et al. (1993) have already pointed out the correlation between flushing episodes with periods of enhanced plume activities in the upper mantle. In Fig. 6 are shown the  $dT/dz$  and  $T$  profiles during the flushing event for the case with two depth-dependent properties shown in Fig. 5. The presence of the negative temperature gradient in the last panel again reflects the spreading of cold material at the base of the mantle. There is not much difference in the profiles between the single depth-dependent case (Fig. 4) and the double depth-dependent case (Fig. 6).

#### 3.4. Depth-dependent expansivity, viscosity and thermal conductivity

The final depth-dependent property we have considered is that of thermal conductivity. Using elementary phonon theory in solid-state physics (Anderson, 1987), it can be shown that there can

be a significant increase in the thermal conductivity from the overburden pressure. We have taken a rather modest increase of a factor of 2.8 (see Eq. (28)) owing to the phonon contribution. Conceivably, the radiative contribution to thermal conductivity could be much greater than the phonon contribution. This would entail incorporation of a nonlinear temperature-dependent form for the thermal conductivity (e.g. Stacey, 1992). For now we will focus on the depth de-

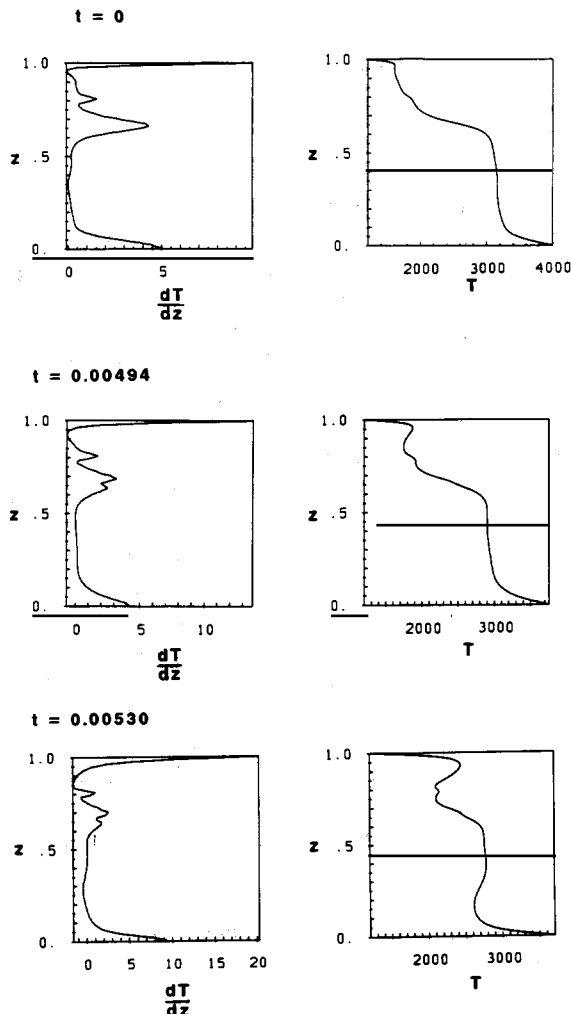


Fig. 8. Profiles of horizontally averaged temperature and temperature gradient of the initial flow and two of the time-steps shown in Fig. 7. Similar behaviour to that in the other two cases (Figs. 4 and 6) is found.

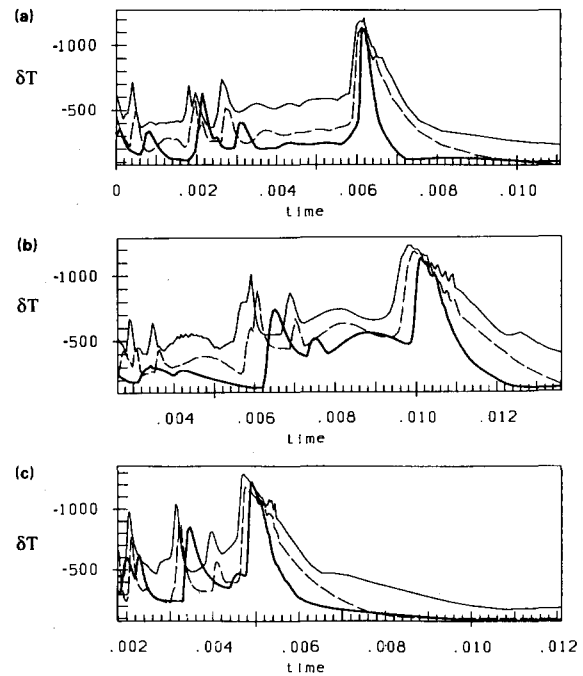


Fig. 9. Time-series of the maximum cold anomalies  $\delta T(z)_{\max}$  at  $z = 0.1025$  (heavy lines),  $z = 0.32$  (dashed lines) and  $z = 0.5$  for depth-dependent expansivity (a), depth-dependent expansivity and viscosity (b), and depth-dependent expansivity, viscosity and thermal conductivity (c). (Note that the timescales for all three cases are roughly the same.)

pendence of thermal conductivity. To the previous model shown in Figs. 5 and 6, we have now added the depth dependence of thermal conductivity. The initial condition was taken from a layered state at  $Ra_0 = 10^8$ . The solution was then integrated with the time-dependent boundary condition for the temperature owing to core cooling. The transitional Rayleigh number  $Ra_0$  at which the flush event took place was found to be around  $2.2 \times 10^7$  ( $\langle Ra \rangle = 8.1 \times 10^5$ ). Thus the transitional surface Rayleigh number increases with additional depth-dependent properties. The mean Rayleigh number, though, decreases for two and then remains almost the same for three depth dependences. The pace of the flushing event (Fig. 7) is about 1.7 times slower than in the case with a single depth dependence (Figs. 3, 4 and 9), but quicker than in the case with two depth dependences. The time of the flush event

shown in the panels of Fig. 7 was around 50 Myr. Colder anomalies were produced than for the previous case with two depth dependences (compare Figs. 5 and 9). Some of the cold anomalies exceeded 1200 K (see second frame of Fig. 7). The magnitude of the hot anomalies were around 100 K higher than in the other two cases with depth-dependent properties (see Figs. 3 and 5). The same scenario of the hot plume erupting in response to the flush event was also found for the case with the triple depth dependences. Both the shorter timescale of the 'flushing' event and the larger magnitude of cold anomalies in comparison with the case with two depth dependences can be explained by the fact that the lower mantle is 100–200 K hotter owing to the increase of thermal conductivity with depth (Fig. 8). Thus the cold masses trapped in the transition zone drop more rapidly and produce colder anomalies which in turn diffuse faster, owing to the high conductivity in the deep mantle. In Fig. 8, we show the horizontally averaged  $dT/dz$  and  $T$  from the initial condition to the last time-frame shown. The profiles do not change much from those for the other two cases (Figs. 4 and 6). The development of a negative temperature gradient at the bottom is a common characteristic in the aftermath of a flush event. The erosion of the peak in  $dT/dz$  in the transition zone is also a sign of the breakdown of layered convection, shown at  $t = 0$ .

#### 4. Discussion and conclusions

The phenomenon of flush instabilities has received great impetus in the past year. The parameter space in this problem, like most problems in mantle convection, is extremely wide. After the initial identification of this phenomenon and the basic physics, it is now essential to (1) explore additional complications of the physics, (2) extend the range of the convective vigour and (3) study the influence of geometry. We have focused on point (1) in this study. The results presented here have shown that colder anomalies in the deep mantle generally can be produced by additional depth-dependent properties. The timescales of the flush process are found to be length-

ened by the introduction of depth-dependent viscosity and shortened again by depth-dependent thermal conductivity. This can partly be explained on the basis of a decrease in the effective Rayleigh number in the deep mantle, and partly by the increase of lower-mantle temperature as a result of enhanced thermal conductivity. Depth-dependent properties also focus hot anomalies into robust upwellings. Hansen et al. (1993) explained this focusing effect by the local increase of buoyancy of a rising plume. This effect is not found for constant-viscosity models with phase transitions (Machtel and Weber, 1991; Zhao et al., 1992; Weinstein, 1993). The focusing effect of the upwelling can impose a profound degree of long-range order on the large-scale circulation. In 3D models of Honda et al. (1993) and Reuteler et al. (1994) these large plumes act as a large attractor, toward which other secondary plumes are drawn. Results based on axisymmetric calculations with temperature- and depth-dependent rheology (Leitch et al., 1992) have shown that the robustness of the major plumes remains with the addition of temperature-dependent viscosity to the other depth dependences of the model.

In our model the surface temperature considered was relatively high. Using a surface temperature of 300–400 K certainly would increase the magnitude of the cold anomalies at the bottom. The effect of sphericity is to focus the cold anomalies at the bottom, as the surface area is around 3.5 times smaller at the CMB than the surface area at 670 km depth. Thus lower surface temperature will produce colder thermal anomalies and spherical geometry will preserve them for a longer time. We can regard these results as a lower bound to the maximum possible strength of the cold anomalies. What we have shown here with this simple 2D model is that cold anomalies can be brought down within 20–50 Myr to the base of the mantle and can remain cold for a long time because of the coherent nature of the instability. Preliminary results with a purely temperature-dependent viscosity have shown that there is a greater tendency toward layering as a result of mechanical decoupling in the transition zone (Steinbach and Yuen, 1993). The fact that there is only one flushing event seems to be character-

istic for our model. We have also found that with larger aspect ratios and in three dimensions there can be more than one flushing event. In conjunction with recent work on converting seismic anomalies to thermal anomalies with mineral physics data (Cadek et al. 1994), these numerical simulations seem to give support to the feasibility of the dump mechanism operating in the Cretaceous period, when subduction rates were very high and large-scale volcanism was prevalent in the western Pacific (Larson, 1991). This type of catastrophic mechanism has important ramifications for the commonly held idea of the steady-state nature of slab dynamics.

### Acknowledgements

We thank Ulli Hansen for discussions and encouragement, and L.M. Weyer for technical assistance. We also thank an anonymous reviewer for his stimulating comments. This research has been supported by the Geochemistry program at NSF, NASA, the Von Humboldt Stiftung of Germany and the Deutsche Forschungsgemeinschaft.

### References

- Anderson, D.L., 1987. A seismic equation of state II. Shear properties and thermodynamics of the lower mantle. *Phys. Earth Planet. Inter.*, 45: 307–323.
- Balachandar, S., Yuen, D.A. and Reuteler, D., 1992. Time-dependent three-dimensional compressible convection with depth-dependent properties. *Geophys. Res. Lett.*, 19: 2247–2250.
- Balachandar, S., Yuen, D.A. and Reuteler, D., 1993. Viscous and adiabatic heating effects in three-dimensional compressible convection at infinite Prandtl number. *Phys. Fluids*, A5(11): 2938–2945.
- Buffett, B.A., Huppert, H.E., Lister, J.R. and Woods, A.W., 1992. Analytical model for solidification of the Earth's core. *Nature*, 356: 329–330.
- Cadek, O.P., Yuen, D.A., Steinbach, V., Chopelas, A. and Matyska, C., 1994. Lower-mantle thermal structure deduced from seismic tomography, mineral physics and numerical modelling. *Earth Planet. Sci. Lett.*, 121: 385–402.
- Chopelas, A. and Boehler, R., 1992. Thermal expansivity of the lower mantle. *Geophys. Res. Lett.*, 19: 1983–1986.
- Christensen, U. and Yuen, D.A., 1985. Layered convection induced by phase-transitions. *J. Geophys. Res.*, 90: 10291–10300.
- Davies, G.F., 1980. Thermal histories of convective Earth models and constraints on radiogenic heat production in the Earth. *J. Geophys. Res.*, 85: 2517–2530.
- Hansen, U. and Ebel, A., 1984. Experiments with a numerical model related to mantle convection: boundary-layer behaviour of small and large scale flows. *Phys. Earth Planet. Inter.*, 36: 374–390.
- Hansen, U., Yuen, D.A. and Kroening, S.E., 1991. Effects of depth-dependent thermal expansivity on mantle circulations and lateral thermal anomalies. *Geophys. Res. Lett.*, 18: 1261–1264.
- Hansen, U., Yuen, D.A., Kroening, S.E. and Larsen, T.B., 1993. Dynamical consequences of depth-dependent thermal expansivity and viscosity on mantle circulations and thermal structure. *Phys. Earth Planet. Inter.*, 77: 205–223.
- Honda, S., Yuen, D.A., Balachandar, S. and Reuteler, D., 1993. Three-dimensional instabilities of mantle convection with multiple phase transitions. *Science*, 259: 1308–1311.
- Ito, E. and Takahashi, E., 1989. Postspinel transformations in the system  $Mg_2SiO_4-Fe_2SiO_4$  and some geophysical implications. *J. Geophys. Res.*, 94: 10637–10646.
- Ito, E., Akaogi, M., Topor, L. and Navrotsky, A., 1990. Negative pressure–temperature slopes for reactions forming  $MgSiO_3$  perovskite from calorimetry. *Science*, 249: 1275–1278.
- Larson, R.L., 1991. Latest pulse of the Earth: evidence for a mid-Cretaceous superplume. *Geology*, 19: 547–550.
- Leitch, A.M. and Yuen, D.A., 1991. Compressible convection in a viscous Venusian mantle. *J. Geophys. Res.*, 96(E1): 15551–15562.
- Leitch, A.M., Yuen, D.A. and Lausten, C.L., 1992. Axisymmetric spherical shell models of mantle convection with variable properties and free and rigid lids. *J. Geophys. Res.*, 97: 20899–20923.
- Machetel, P. and Weber, P., 1991. Intermittent layered convection in a model mantle with an endothermic phase change at 670 km. *Nature*, 350: 55–57.
- Reuteler, D.M., Yuen, D.A., Balachandar, S. and Honda, S., 1994. Three-dimensional mantle convection: effects of depth-dependent properties and multiple phase transitions. *Int. Video J. Eng. Res.*, in press.
- Ricard, Y., Spada, G. and Sabadini, R., 1993. Polar wandering of a dynamic Earth. *Geophys. J. Int.*, 113: 284–298.
- Richter, F.M., 1973. Finite amplitude convection through a phase boundary. *Geophys. J. R. Astron. Soc.*, 35: 265–276.
- Sharpe, H.N. and Peltier, W.R., 1978. Parameterized mantle convection and the Earth's thermal history. *Geophys. Res. Lett.*, 5: 737–740.
- Solheim, L.P. and Peltier, W.R., 1994. Avalanche effects in phase transition modulated thermal convection: a model of the Earth's mantle. *J. Geophys. Res.*, in press.
- Spada, G., Sabadini, R., Yuen, D.A. and Ricard, Y., 1992. Effects on postglacial rebound from the hard rheology in the transition zone. *Geophys. J. Int.*, 109: 683–700.

- Stacey, F.D., 1992. *Physics of the Earth*, 3rd edn. Brookfield Press, Brisbane, Queensland.
- Steinbach, V. and Yuen, D.A., 1992. Convection with phase transitions and temperature-dependent viscosity. *EOS Trans. Am. Geophys. Union*, 74(6): 300.
- Steinbach, V., Hansen, U. and Ebel, A., 1989. Compressible convection in the Earth's mantle: a comparison of different approaches. *Geophys. Res. Lett.*, 16: 633–636.
- Steinbach, V., Yuen, D.A. and Zhao, W., 1993. Instabilities from phase transitions and the timescales of mantle thermal evolution. *Geophys. Res. Lett.*, 20: 1119–1122.
- Su, S. and Dziewonski, A.M., 1992. On the scale of mantle heterogeneity. *Phys. Earth Planet. Inter.*, 74: 29–54.
- Tackley, P.J., Stevenson, D.J., Glatzmaier, G.A. and Schubert, G., 1993. Effects of an endothermic phase transition at 670 km depth in a spherical model of convection in the Earth's mantle. *Nature*, 361: 699–704.
- Turcotte, D.L., Torrance, K.E. and Hsui, A.T., 1973. Convection in the Earth's mantle. In: S. Fernbach (Editor), *Methods in Computational Physics*, Vol. 12. Academic Press, New York, pp. 431–454.
- Weinstein, S.A., 1993. Catastrophic overturn in the Earth's mantle driven by multiple phase changes and internal heat generation. *Geophys. Res. Lett.*, 20: 101–104.
- Yuen, D.A., Cadek, O., Chopelas, A. and Matyska, C., 1993. Geophysical inferences of thermal–chemical structures in the lower mantle. *Geophys. Res. Lett.*, 20: 899–902.
- Zhao, W., Yuen, D.A. and Honda, S., 1992. Multiple phase transitions and the style of mantle convection. *Phys. Earth Planet Inter.*, 72: 185–210.